Biophysical *Journal*
Article

Biophysical Society

Impact of chromosomal organization on epigenetic drift and domain stability revealed by physics-based simulations

Joseph G. Wakim,[1] Sarah H. Sandholtz,[2] and Andrew J. Spakowitz[1,3,4,5,*]
[1]Department of Chemical Engineering, [2]Department of Chemistry, [3]Department of Materials Science and Engineering, [4]Biophysics Program, and [5]Department of Applied Physics, Stanford University, Stanford, California

ABSTRACT We examine the relationship between the size of domains of epigenetic marks and the stability of those domains using our theoretical model that captures the physical mechanisms governing the maintenance of epigenetic modifications. We focus our study on histone H3 lysine-9 trimethylation, one of the most common and consequential epigenetic marks with roles in chromatin compaction and gene repression. Our model combines the effects of methyl spreading by methyltransferases and chromatin segregation into heterochromatin and euchromatin because of preferential heterochromatin protein 1 (HP1) binding. Our model indicates that, although large methylated domains are passed successfully from one chromatin generation to the next, small alterations to the methylation sequence are not maintained during chromatin replication. Using our predictive model, we investigate the size required for an epigenetic domain to persist over chromatin generations while surrounded by a much larger domain of opposite methylation and compaction state. We find that there is a critical size threshold in the hundreds-of-nucleosomes scale above which an epigenetic domain will be reliably maintained over generations. The precise size of the threshold differs for heterochromatic and euchromatic domains. Our results are consistent with natural alterations to the epigenetic sequence occurring during embryonic development and due to age-related epigenetic drift.

SIGNIFICANCE Epigenetic marks enable cells with the same genetic code to express a broad array of phenotypes by dictating chromatin structure, which modulates transcription and gene expression. During chromatin replication, the epigenetic sequence is temporarily disrupted as marks are randomly distributed between daughter strands. Reestablishment of the epigenome following replication is necessary to ensure maintenance of cell identity. Our work applies a physics-based model of chromatin compaction and epigenetic mark conferral to identify patterns affecting histone H3 lysine-9 trimethylation heredity. We identify a threshold epigenetic domain size required for persistent maintenance of the epigenome during chromatin replication. Our results are consistent with dynamic patterns in the epigenome expected during embryonic development and with aging, implicating chromatin looping as an underlying mechanism in both processes.

INTRODUCTION

All cells within an organism contain the same genetic material but exhibit a wide variety of characteristics and functions. This diversity arises not because of differences in the sequence of DNA basepairs but because of epigenetics: chemical modifications to chromosomal DNA and post-translational modifications to DNA-associated proteins that modulate gene expression. Cell development and differentiation illustrate the crucial role epigenetics plays in gene regulation as a determinant of which genes are expressed at what time. Abnormal patterns of epigenetic marks disrupt typical gene expression and are associated with many prevalent diseases, including cancer, diabetes, obesity, and developmental disorders (1–3).

Nucleosomes, which consist of DNA wrapped approximately one and a half times around a set of eight histone proteins, are the fundamental unit of chromosomal DNA and are responsible for its structure. Epigenetic modifications to the tails of histone proteins govern the local and global organization of chromatin. By modulating the spatial

Submitted May 28, 2021, and accepted for publication October 18, 2021.
*Correspondence: ajspakow@stanford.edu
Joseph G. Wakim and Sarah H. Sandholtz are co-first authors.
Editor: Lars Nordenskiöld
https://doi.org/10.1016/j.bpj.2021.10.019

arrangement of the chromosomes, epigenetic marks affect the accessibility of genes to transcription factors and thereby regulate gene expression. During interphase, DNA segregates into densely packed, less transcriptionally accessible regions of heterochromatin and loosely packed, more transcriptionally accessible regions of euchromatin. Histone methylation is required for the formation of heterochromatin (4) and gene repression (5–7).

Heterochromatin protein 1 (HP1) binds specifically to histone H3 lysine-9 (H3K9) (8–10) and oligomerizes when bound to adjacent nucleosomes, causing compaction (11,12). Epigenetic methyl marks interact with HP1, which shows the strongest affinity for trimethylation (H3K9me3) (8–10). HP1 also interacts cooperatively with the H3K9 methyltransferases SUV39H1/2 (13–15), which spread methyl marks to unmethylated nucleosomes in spatial proximity. Chromatin contact experiments reveal a connection between chromatin organization and epigenetic regulation, as contact maps show distinct patterns that correlate with the profiles of epigenetic modifications (16,17).

The epigenetic sequence must be passed faithfully to daughter cells to ensure continuity of proper cellular identity and behavior. During replication, the histone methylation level is temporarily diluted by a factor of two, as parental nucleosomes are placed randomly on one of the two daughter strands. The gaps between parental nucleosomes are filled with newly synthesized, unmarked nucleosomes (18), and the histone methylation level gradually increases during the cell cycle to return to its original level (19,20).

A "buffer model" has been proposed to explain both the imprecise inheritance of histone methylation at individual nucleosomes and the consistency of gene silencing at genomic scales (19). Theoretical models show that establishing robust bistability requires cooperativity and long-range interactions between nucleosomes (21–24). Models that include physically motivated chromatin connectivity reproduce experimental observations of the extent of epigenetic spreading and further demonstrate that coupling between three-dimensional structure and one-dimensional epigenetic spreading promotes bistability and epigenetic memory (25–27). Although some models find that boundary elements are necessary to restrict epigenetic marks to a local domain (27–29), others find that barrier-free mechanisms, such as the random diffusive motion of both the chromatin fiber and a chromatin-bound enzyme (30) or the HP1-driven phase segregation into heterochromatin and euchromatin (31), capture the formation and maintenance of epigenetic domains.

Micheelsen et al. develop analytical approaches to study the stability of the epigenetic profile across cell divisions. They find that a positive feedback mechanism for nucleosome modification is robust against the temporary destabilization caused by cell division. They also observe that faster rates of cell division lead to more frequent stochastic transitions between epigenetic states and that the stability of a distinct epigenetic domain is proportional to its size (22). In their stochastic study of various epigenetic circuits, Sneppen and Dodd include a replication step in which nucleosomes randomly lose their epigenetic marks, and they note that multiple possible circuits can establish epigenetic stability (32). Similarly, Zerihun et al. utilize a stochastic model to study the dynamics of the epigenetic state after replication, which they imitate by periodically diluting the epigenetic mark density. They discover that the epigenetic state is more sensitive to fluctuations immediately after replication and that the length of the cell cycle has a significant impact on epigenetic memory (33).

Although the histone methylation level reestablishes itself after each replication event, over the course of an organism's whole lifetime, both the epigenetic profile and features of the chromatin structure evolve (34), shifting farther from their original state. Such age-related changes in the epigenetic profile, termed epigenetic drift, can contribute to impaired cellular functions. It has been broadly observed that as organisms age, their chromatin becomes more euchromatic and transcriptionally active (35). In fact, changes in heterochromatin correlate with aged phenotypes across multiple species, including *Caenorhabditis elegans*, *Drosophila*, and humans (36–38). For instance, human cells from patients with Hutchinson-Gilford progeria syndrome, a genetic condition that results in premature aging, show a decrease in H3K9me3 levels, a reduction in association of HP1 with pericentrosomal DNA, and a reduction in heterochromatin (35,39). Embryonic stem cells from a model system of Werner syndrome, another premature aging disorder, similarly show loss of H3K9me3, HP1, and SUV39H1 (38). Based on such findings and noted cross-species commonalities, the proposed "loss of heterochromatin" model suggests that a reduction in heterochromatin is a driving feature of aging (35,40). Indeed, the organization of the genome, and not simply the abundance of epigenetic marks, appears to have a significant effect on aging, as evidenced by reports of a shift in the distribution of H3K9me3 from heterochromatin to euchromatin and an overall increase in H3K9me3 in aged *Drosophila* (41).

We employ our theoretical model for the reestablishment of epigenetic modifications following DNA replication to explore the relationship between domain size and epigenetic stability for both heterochromatic and euchromatic domains. Based on our current understanding of heterochromatin/euchromatin segregation and methylation spreading (42,43), our model incorporates the relationship between methylation state and HP1 binding as well as the cooperative interaction between HP1 and methyltransferase. Our model predicts the organization of chromosomal DNA based on the cooperative interactions between bound HP1, resulting in a condensed heterochromatin phase that resembles an "inverted" nucleus (44) (discussed further in Materials and methods) but nonetheless captures contact

frequencies found from Hi-C measurements (42). Our previous work shows that small euchromatic and heterochromatic domains cannot maintain their original methylation level and are gradually consumed by larger domains of the opposite compaction state (31).

At a large enough size, however, one would expect that an epigenetic domain could persist despite being surrounded by a larger antagonistic region. By artificially demethylating a segment in a region of high methylation and artificially methylating a segment in a region of low methylation, we aim to observe the critical size necessary for a segment to survive within a larger region of the opposite compaction state. Our results indicate that the epigenetic sequence is more susceptible to aberrations of overmethylation than to those of undermethylation, suggesting that the cell might operate under conditions that slightly favor demethylation and the formation of euchromatin. Our finding that the system is more robust against loss of methylation is consistent with experimental observations that epigenetic drift tends to be in the direction of loss of H3K9me3 and heterochromatin. Thus, our model reveals further biophysical detail about the relationship between epigenetic regulation and chromatin organization and holds relevance for changes to the epigenetic sequence that occur as a result of normal recombination events, age-related epigenetic drift, and artificial manipulations. Interventions that are designed to selectively activate or repress a specific gene may entail relocating that gene to drive it from heterochromatin into euchromatin or vice versa and thereby affect its transcriptional activity. Understanding the conditions required for the stability of epigenetic domains is therefore critical to predicting the chromosomal tolerance for such potential genetic relocations.

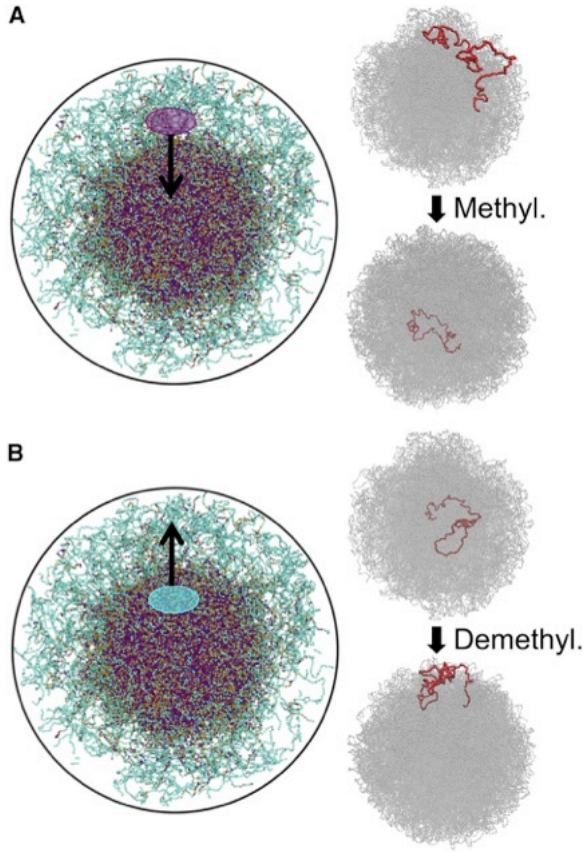

FIGURE 1 Artificial methylation and demethylation cause nucleosome migration between heterochromatic and euchromatic phases. (*A*) Following artificial methylation, nucleosomes originally located in a loosely packed, peripheral euchromatic domain tend to move into a dense heterochromatic core due to increased HP1 binding and favorable HP1 oligomerization. (*B*) Conversely, after removing methyl marks from nucleosomes in heterochromatin, these nucleosomes tend to move into the surrounding euchromatic domain due to less favorable HP1 binding to unmethylated nucleosomes. Subplots include schematics illustrating the general direction of nucleosome migration following artificial methylation (*A*, *left*) or demethylation (*B*, *left*), where nucleosomes in cyan, gold, and magenta are classified in euchromatic, boundary, and heterochromatic domains, respectively. To exemplify this, each subplot also highlights the location of 300 nucleosomes in red before and after artificial methylation (*A*, *right*) or demethylation (*B*, *right*).

MATERIALS AND METHODS

We leverage our model for the heritability of the methylation sequence, which integrates two fundamental processes of chromatin compaction and methyl spreading (31). Our aim in this work is to identify the conditions under which an artificially demethylated heterochromatic region will migrate into euchromatin and vice versa, as the schematic in Fig. 1 illustrates. We begin with an experimentally derived profile of H3K9me3 for human chromosome 16. We then artificially methylate or demethylate a continuous segment of nucleosomes in euchromatin or heterochromatin, respectively, producing a chromosome that we label with "generation zero." We assume the H3K9me3 profile to be fixed until chromosomal replication takes place. Assuming that structural equilibration occurs faster than chromosomal replication, we model equilibrium chromatin organization by Metropolis Monte Carlo (MC) simulation. From these simulations, we collect an ensemble of equilibrium configurations that we use to quantify local chromatin compaction. We use local chromatin compaction as an input to our kinetic model of loop-mediated epigenetic mark conferral, which we evaluate to generate a new H3K9me3 profile predicting the chromosome's updated epigenetic state following replication. The chromosome with the updated H3K9me3 profile is labeled with "generation one." By iterating between MC structural prediction and the kinetic model of loop-mediated mark conferral, we predict H3K9me3 profiles and chromatin structures following four chromosome replication cycles, until modeling the chromosome at "generation four."

Chromatin modeled as a wormlike chain

We simulate human chromosome 16 and represent each of its 393,216 nucleosomes as an individual bead. Such large-scale simulations necessitate a coarse-grained approach, so we use the discrete, stretchable, shearable wormlike chain model, which both captures the energetics of a semiflexible polymer and allows for more coarse discretization. The discrete, stretchable, shearable wormlike chain model is described in detail in the Supporting materials and methods Appendix for (42) and in the original articles in which it was developed (45–47). We model chromatin as having the same persistence length of bare DNA, with nucleosomes spaced 50 bp apart.

To mimic the confinement DNA experiences in the nucleus, we set a spherical confinement around the single chromosome in our simulation. This confinement is 1.8μm in diameter, corresponding to the approximate size of a chromosome territory (48). To calculate the total interaction free energy between chromosomal segments, we divide the system into cells of volume Δ^3 and define ϕ_c as the volume fraction of chromatin calculated inside discrete bins of width Δ. As in (49), we use linear density interpolation to calculate ϕ_c for each cell. We define the interaction free energy to be

$$F_{int}(\phi_c) = \begin{cases} \chi\Delta^3\phi_c^2 & \text{if } \phi_c < 0.5 \\ \infty & \text{otherwise.} \end{cases}$$

We set $\Delta = 28.7$nm to capture density fluctuations on an appropriate length scale for nucleosome-level detail. We assign each bead a volume of 520nm^3 to correspond to the approximate volume of a nucleosome. We choose a moderate value of the parameter χ that is large enough to prevent the formation of chromatin-less regions, but not so large as to prevent noticeable variation in chromatin density. We note that this coarse-grained binning procedure does not prohibit the overlap of individual nucleosomes. However, no bin is allowed to be more than 50% full of nucleosomes. This method is appropriate for revealing equilibrium density fluctuations in chromatin on length scales greater than Δ.

The total energy of the system includes energy from polymer-chain deformation, nonspecific repulsion, and HP1 binding: $E = E_{poly} + \sum_{bins} F_{int}(\phi_c) + E_{bind}$. We select configurations from an ensemble of the system using MC sampling.

MC structural prediction

Our model for chromatin compaction predicts DNA segregation into heterochromatin and euchromatin based on a fixed methylation sequence and cooperative HP1 binding (42). We use a polymer-based MC simulation to sample configurations from the equilibrium ensemble of this system. Our simulations include five categories of moves that 1) rotate a segment of the polymer about the axis that runs through its ends, 2) change the binding state of histone tails, 3) rotate a single bead, 4) translate beads, and 5) pivot the end of the chain. Moves are performed repeatedly in order for the system to reach equilibrium. We use parallel tempering between different chemical potentials (i.e., concentrations of HP1) to ensure that full sampling of the configuration space can occur. Our model does not include any topological constraints on the DNA. By implementing a coarse-graining interaction (49), we simulate the entire human chromosome 16 with nucleosome-scale discretization.

Based on the experimentally observed connection between HP1 and methyltransferase (50,51), we incorporate HP1 binding directly into our model. We allow HP1 to bind and unbind to both methylated and unmethylated histone tails, adjusting for the preferential binding of HP1 to methylated tails. Based on experimental data from Canzio et al. (11) and modeling by Mulligan et al. (52), we set the methylated and unmethylated histone-HP1 binding affinities to $\varepsilon_M = -0.01k_BT$ and $\varepsilon_U = 1.52k_BT$, respectively. To account for the oligomerization of HP1, which leads to compaction of the chromosome, our model also includes an experimentally based energetic benefit for regions with higher concentrations of HP1 (11). HP1-bound nucleosomes that come within an interaction radius experience a $J = -4.0k_B$T free-energy benefit. We choose an interaction radius of $r_{int} = 3$nm to correspond to the approximate length of a histone tail (53). We use a two-state model in which each H3 tail is either bound by HP1 or not bound. The free concentration of HP1 determines the chemical potential through the relation $\mu = k_B T \log([\text{HP1}]_{\text{free}})$. We use the canonical ensemble (i.e., fixed number) for the DNA and nucleosomes and the grand canonical ensemble (i.e., fixed chemical potential) for the HP1 molecules. We calculate the interaction between separate nucleosomes based on ρ, the local number density of bound HP1 interpolated from a linear grid with spacing Δ. Altogether, the HP1-binding energy is given by

$$E_{\text{bind}} = \sum_{i=1}^{N}\left[J'\sigma_i^1\sigma_i^2 + \sum_{j=1}^{2}(\varepsilon_i^j - \mu)\sigma_i^j\right] + \sum_{\text{bins}}\frac{1}{2}Jv_{int}\Delta^3\rho^2,$$

where $v_{int} = (4/3)\pi r_{int}^3$ denotes the interaction volume, N is the number of nucleosomes, σ_i^j is 1 if the jth H3 tail of the ith nucleosome is bound by HP1 and 0 otherwise, ε_i^j is ε_M or ε_U, depending on the methylation state of the corresponding histone tail, and $J' = J(1 - v_{int}/\Delta^3)$ to correct for double-counted interactions between H3 tails on the same nucleosome (42).

Our model behaves similarly to other models that treat chromatin as a block copolymer (54–56), but our approach incorporates local binding of HP1 that is sensitive to changes in the surrounding epigenetic sequence. Data-driven modeling approaches achieve exquisite agreement with in vivo genomic contact maps based on Hi-C measurements (57,58). Our bottom-up approach predicts many genomic contacts that are measured in Hi-C experiments while maintaining predictive ability for epigenetic mark conferral.

Our MC simulations predict an "inverted" architecture for a single chromosome territory, characterized by a dense heterochromatic core and a loose euchromatic periphery. On the scale of the entire nucleus, such inverted configurations are observed in rods of nocturnal animals (44). Meanwhile, the "conventional" nucleus is defined by an opposite configuration, with heterochromatin preferentially located at the nuclear envelope. To reproduce the organization of the conventional nucleus, a favorable interaction between HP1-bound nucleosomes and the nuclear envelope may be specified (59,60). However, specifying such an interaction with a free parameter may bias our model and compromise predictability. To minimize our use of free parameters, we have chosen not to specify an interaction between HP1-bound nucleosomes and the confining boundary. For structural simulations of a single chromosome territory, predicted configurations with centrally located heterochromatin have reproduced features observed in experimental Hi-C contact maps (42,57,61). Likewise, experimental Hi-C contact maps from conventional and inverted nuclei produce common features and consistent degrees of compartmentalization (44,59). The observations suggest that compartmentalization of heterochromatic and euchromatic domains is independent of the nuclear envelope (59). Therefore, for the purposes of predicting HP1-bound nucleosome contacts and associated loop-mediated H3K9me3 conferral to study epigenetic drift and domain stability within a chromosome territory, our simulations are valid without an interaction with the nuclear boundary.

We determine the original methylation profile from experimental ChIP-seq data (62,63). Histone tails are methylated by applying a cutoff to the ChIP-seq signal such that ~50% of the histone tails are methylated. We calculate the fraction of methylated nucleosomes in sliding windows of 101 nucleosomes centered around each nucleosome and refer to this measure as the "methylation state." This approach is based on the finding that the methylation level of a region of ~100 nucleosomes is a better predictor of local compaction state (i.e., located in heterochromatin or euchromatin) than an individual nucleosome's methylation state (42). We apply the same cutoffs for window-averaged methylation established in previous work (31) to identify the compaction state of each nucleosome and identify the longest continuous heterochromatic and euchromatic regions of the chromosome. At the center of the heterochromatic and euchromatic regions, a segment of the original methylation sequence is replaced with a segment that is completely unmethylated or completely methylated, respectively. The size of the altered segment is varied (from as small as 10 nucleosomes to as large as 600 nucleosomes) to examine the relationship between domain size and epigenetic stability. We label chromosomes with the directly altered methylation profiles as belonging to "generation zero."

Kinetic model of epigenetic mark conferral

Our methylation model predicts, based on the spatial arrangement of the chromatin, which nucleosomes become methylated through loop-mediated

spreading (43). Experimental measurements of methyl spreading around a nucleosome (50,51) inform the function of the methyltransferase in our model. Given the interaction between HP1 and methyltransferase, methylation is able to spread from both methylated and unmethylated nucleosomes as long as HP1 is bound. However, spreading will occur differentially from methylated and unmethylated nucleosomes as a result of their different binding affinities for HP1 (11). For each snapshot of chromatin structure produced by MC simulation, we quantify compaction at each nucleosome i by the number of surrounding HP1-bound nucleosome tails within cutoff distance $a = 15$ nm. We assign this quantity to n_{HP1_i}-labeled "near-neighbor count" or "neighbors." As with our previous work, we choose the 15-nm cutoff distance to represent approximately half the resolution of the MC simulation. We average the number of HP1-bound tails within a cutoff distance a of the ith nucleosome over 26 independent, equilibrated chromatin structures, which we denote by $\langle n_{\mathrm{HP1}_i} \rangle$. The average number of near neighbors at each nucleosome position provides a representative map of nucleosome connectivity.

We write a kinetic equation for the change in methylation probability with respect to time $\frac{dp_i}{dt} = k_m^{(0)} \langle n_{\mathrm{HP1}_i} \rangle (1 - p_i) - k_d p_i$, where p_i is the probability that the ith nucleosome is methylated (i.e., trimethylated in our model), $k_m^{(0)}$ is the bare methyltransferase rate, and k_d is the demethylation rate. We constrain our rate constants to the parameter $\alpha_d = k_m^{(0)} / k_d$, the relative rate of methylation to demethylation. Consistent with previous work (31), we set $\alpha_d = 0.042$. This value for α_d ensures that the fraction of methylated nucleosomes returns to approximately the same value after each successive generation for a moderate concentration of unbound HP1 (0.700 μM), which we previously identified as an optimal concentration for maintaining the epigenetic sequence (31). In this work, we focus on this optimal concentration of HP1 to explore the domain size requirements for epigenetic stability under the most beneficial conditions for epigenetic memory. Using local chromatin compaction as an input for the methyl spreading master equation, we solve for the steady-state methylation profile. The methylation status of each nucleosome is selected based on the probabilities p_i from the master equation. The resulting methylation sequence then serves as input for the next MC simulation for chromatin organization. Because the updated methylation sequence models the H3K9me3 profile of the chromosome after a replication cycle, we label the chromosome with this sequence as belonging to the next generation (e.g., "generation one" through "generation four").

Model of H3K9me3 mark heritability

We integrate our models for chromatin organization and methyl spreading by alternating between MC simulations for the three-dimensional configuration and a master equation solution for the methylation sequence (31). By iterating between chromatin compaction steps and methyl-spreading steps, we observe the evolution of chromatin structure and epigenetic sequence over multiple generations. One generation is defined to be one MC simulation coupled with one master equation solution. Fig. 2 shows snapshots for three values of the artificially demethylated region (120, 150, and 180 nucleosomes) for chromatin generations zero, two, and four. The artificially demethylated region is highlighted in these images, and the view of the simulation is rotated such that the center of mass of the artificially demethylated region is aligned along the x axis. Therefore, the radial position of the demethylated region is clearly identified in the snapshots of Fig. 2.

Experimental measurements of the rate of transfer of histone methylation, methyltransferase activity, and the diffusion coefficient of genetic loci in mammalian cells suggest that chromosomal dynamics are much faster than methylation dynamics (64–66), and our choice of using an averaged nucleosome connectivity reflects this difference in timescales. An averaged connectivity represents a range of chromosomal structures and

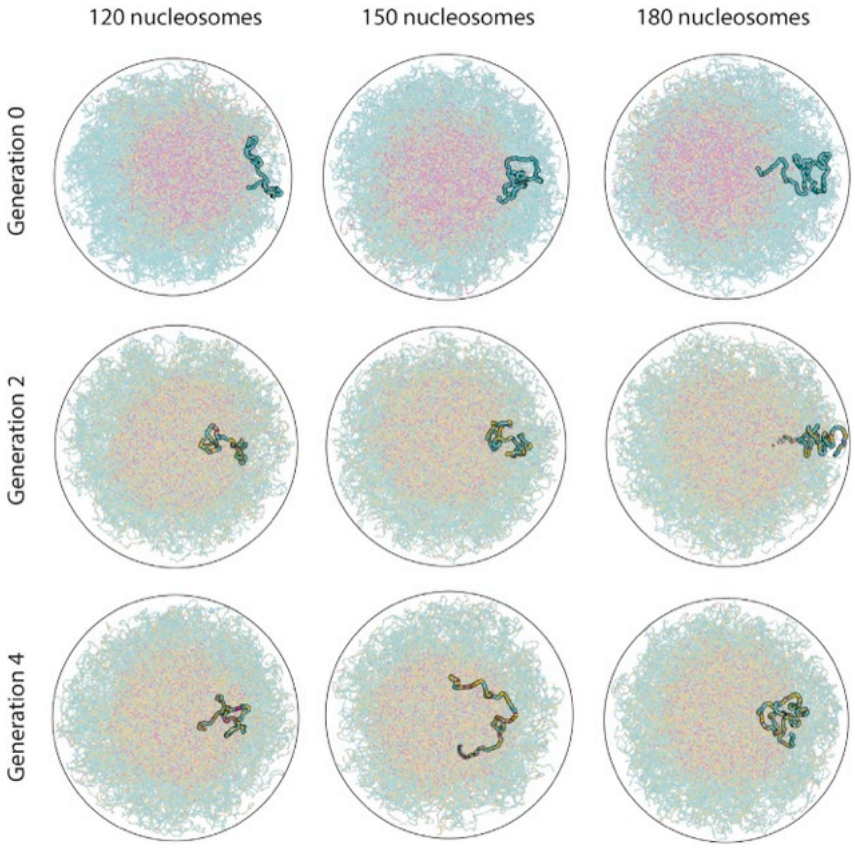

FIGURE 2 Our physics-based simulations depict nucleosome migration between a loose euchromatic periphery and a dense heterochromatic core, reflecting dynamic patterns of H3K9me3 modifications during cell replication. We render snapshots of chromatin organization within a spherical chromosomal territory following artificial demethylation of a variable-length region of heterochromatin. At generation zero, H3K9me3 modifications are artificially removed from segments of 120, 150, and 180 nucleosomes in heterochromatin, causing these nucleosomes to relocate to a peripheral euchromatic domain with other similarly unmethylated nucleosomes. We iterate between MC simulation of chromatin organization and a kinetic model of loop-mediated epigenetic mark conferral to predict the epigenetic profile following four subsequent cycles of chromosomal replication. Snapshots from our simulations collected at chromosome generations two and four (following two and four replication cycles, respectively) depict progressive reestablishment of the methyl sequence and migration of the modified nucleosomes back toward the dense heterochromatic core. The view is rotated such that the center of mass of the highlighted artificially demethylated region is aligned with the x axis for each snapshot.

therefore takes into account local fluctuations in nucleosome positions and HP1 binding. Furthermore, additional analysis demonstrates that the mechanism for epigenetic heritability presented in (31) is robust against variations in the simulation and master equation procedure. Alternative procedures that represent different timescales for chromosomal rearrangement and methylation spreading produce qualitatively consistent results (31) and, therefore, the approach taken in this and prior work is reasonable.

Materials and data availability

MC simulation code to predict chromosomal organization at each generation and code/documentation for the master equation solution for methylation dynamics are found in the Spakowitz Lab GitHub (https://github.com/SpakowitzLab) and on our lab website (http://www.stanford.edu/~ajspakow/).

RESULTS

We perform a series of simulations of the reestablishment of the methylation sequence after DNA replication, as outlined above. These simulations explore how artificially methylated or demethylated regions of chromatin persist over multiple cell cycle generations. We find that there is a critical size threshold between 100 and 200 nucleosomes required for a domain of a particular epigenetic state to survive within a larger region of the opposite state. Domains smaller than the threshold size are absorbed by the larger region and gradually switch epigenetic state, whereas domains larger than the threshold size persist stably over generations and maintain consistent epigenetic states.

Mark spreading reverses minor epigenetic perturbations

To characterize the threshold size above which an epigenetic domain persists during cell replication, we focus our analysis on a linearly adjacent, 1000-nucleosome "local" region containing the artificially adjusted nucleosome segment. We partition this local region into "artificial" and "surrounding" segments, which we separately characterize during later analysis. For each simulated alteration to the epigenome, we plot the evolution of methylation states and near-neighbor counts in the local region following four chromatin replications. These profiles capture the gradual spreading of methylation marks at interfaces between epigenetic domains, blurring the boundaries between condensed heterochromatic and loose euchromatic regions. For short heterochromatic regions established by artificially methylated nucleosomes, spreading of the inserted methylation marks during chromatin replication causes a reversion to the original euchromatic state. Similarly, for short segments of euchromatin caused by artificial demethylation, we observe that mark spreading from surrounding regions restores a continuous, compact heterochromatic domain. For example, Fig. 3 plots the progression of methylation state and near-neighbor count profiles following 150-nucleosome

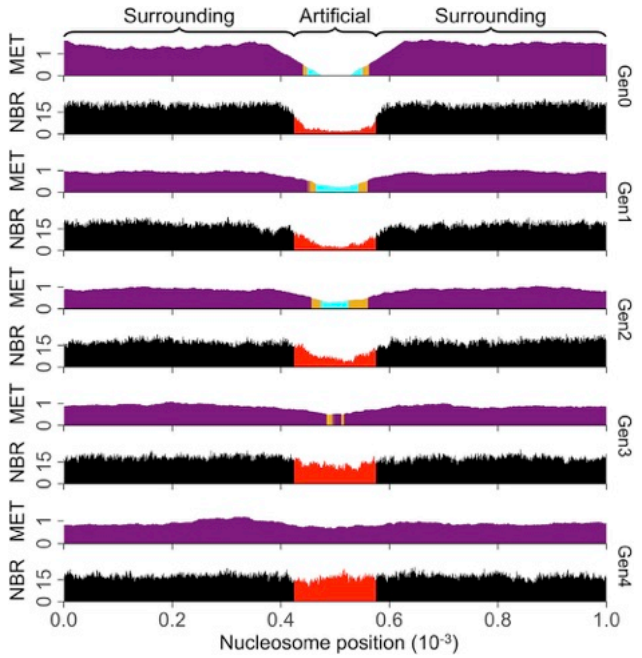

FIGURE 3 We use bar charts to represent the profiles of H3K9 trimethylation ("MET") and near-neighbor counts ("NBR") for a continuous 1000-nucleosome "local" region of the chromosome containing our artificially demethylated domain. At each nucleosome position, the methylation profiles plot the 101-nucleosome window average of the number of histone tails modified with H3K9me3, whereas the neighbor count profiles plot the average number of HP1 proteins bound within a 15-nm cutoff radius among all equilibrated MC snapshots. Beginning with an initial, experimentally derived H3K9me3 profile, we artificially demethylate 150 nucleosomes from a continuous heterochromatic domain and label the resulting chromosome as belonging to generation zero ("Gen0"). We then apply MC simulation to predict the structure of the manipulated chromosome and generate the neighbor count profile. From the neighbor count profiles, we leverage a kinetic model of loop mediated epigenetic mark conferral (43) to predict patterns of H3K9me3 modifications at the next chromosome generation. By iterating between our kinetic model of epigenetic mark conferral and MC structural prediction, we predict the H3K9 trimethylation and neighbor count profiles following four subsequent chromosome replication cycles (labeled chromosome "Gen1" to "Gen4"). The "local" region is divided into "artificial" and "surrounding" subregions for subsequent analyses. In the methylation state profiles, nucleosome positions colored in magenta, gold, and cyan are classified into heterochromatic, boundary, and euchromatic domains, respectively. In the neighbor count profiles, positions colored in red indicate which nucleosomes were artificially demethylated at generation zero. These profiles offer a basis for quantitative comparison of the methylation states and near-neighbor counts in the regions containing and around the artificially modified nucleosomes during progressive cell generations.

artificial demethylation from a continuous heterochromatic domain, illustrating that the original domain is restored after four chromatin replications.

Epigenetic domains persist during chromatin replication beyond a critical length

When the size of an artificially methylated or demethylated nucleosome segment exceeds the threshold length between

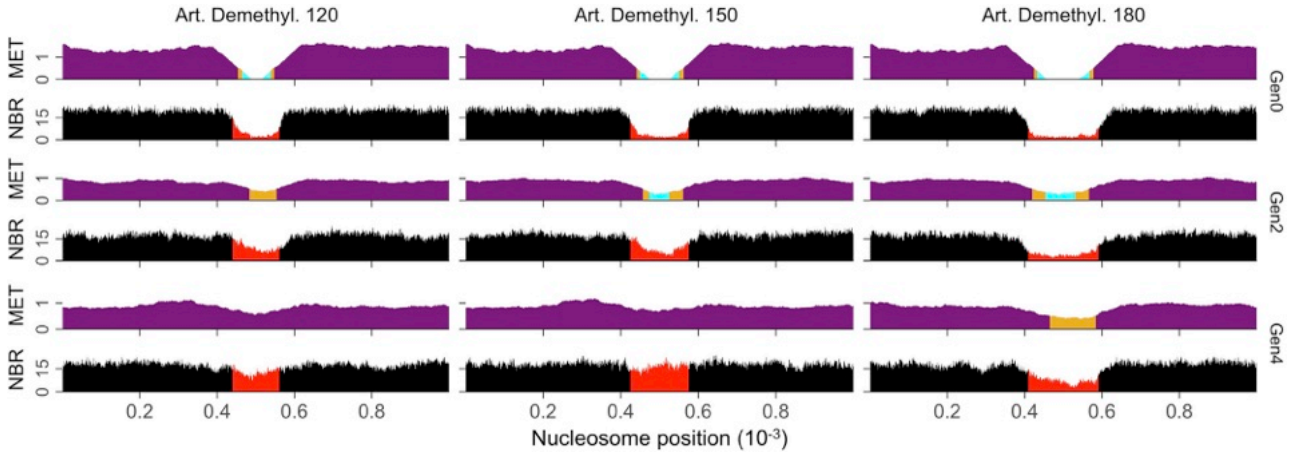

FIGURE 4 We simulate dynamic patterns in the profiles of H3K9 trimethylation ("MET") and nucleosome near-neighbor counts ("NBR") during four chromatin generations following artificial demethylation of a nucleosome segment in heterochromatin. Artificial demethylation of variable-length segments in heterochromatin are introduced to an experimentally derived profile of H3K9me3 for human chromosome 16, and a chromosome with the modified H3K9me3 profile is referred to as "generation zero." We then iteratively simulate chromatin structure and mark conferral to predict similar profiles of H3K9 trimethylation and near-neighbor counts following four subsequent chromosome replication cycles, yielding what we refer to as chromosome "generation one" through "generation four." Here, we plot profiles following artificial demethylation of 120, 150, and 180 nucleosomes at chromosome generations zero ("Gen0"), two ("Gen2"), and four ("Gen4"). In the methylation state profiles, nucleosome positions colored in magenta, gold, and cyan represent heterochromatic, boundary, and euchromatic domains, respectively. In the neighbor count profiles, positions marked in red indicate where H3K9 trimethylation marks were artificially removed during generation zero. Variable-length artificial demethylation reveals a critical perturbation threshold in the hundreds-of-nucleosomes scale required to introduce long-term changes to the H3K9me3 profile. Demethylation of nucleosome segments below this threshold produce transient domains of euchromatin, which revert back to heterochromatin following reestablishment of H3K9me3.

100 and 200 nucleosomes, mark spreading appears insufficient to restore the original epigenetic state within four chromatin generations. Fig. 4 plots methylation state and near-neighbor count profiles for artificially demethylated nucleosome segments around the threshold length, with alterations made to an originally continuous heterochromatic domain. This figure juxtaposes a transient 120-nucleosome epigenetic alteration with a more robust 180-nucleosome alteration. Near the threshold alteration length, as the number of artificially demethylated nucleosomes increases, there is a concomitant increase in the number of chromatin replication cycles required to restore the lost marks and reestablish the heterochromatin domain. When comparing simulations with artificially methylated and demethylated nucleosomes, we observe that fewer methylated nucleosomes are required to establish a persistent epigenetic domain than demethylated nucleosomes (for demonstration, see Fig. S1). As such, heterochromatin appears more robust to perturbations in the epigenome than euchromatin.

We represent the evolution of heterochromatic and euchromatic domains using empirical cumulative distribution functions (eCDFs), which we separately plot for the artificial and surrounding regions. For example, Fig. 5 plots eCDFs of near-neighbor counts at four chromatin generations following artificial methylation and demethylation of 100 nucleosomes from euchromatin and heterochromatin, respectively. Following both methylation and demethylation, the distribution of near-neighbor counts in the surrounding regions quickly stabilizes, whereas that in the artificial region continues to evolve during all chromatin generations. Shifts in the near-neighbor count eCDFs of the artificial region capture the reversion to the epigenetic state of surrounding nucleosomes. Artificially methylated nucleosomes lose neighbors as they loosen into a euchromatic state, whereas artificially demethylated nucleosomes gain neighbors and restore a compact heterochromatin domain.

We quantify changes in methylation state and near-neighbor count distributions between pairs of chromatin generations using the Kolmogorov-Smirnov (KS) test statistic, which gives the greatest distance between two eCDFs. The test statistic is separately calculated for distributions from artificial and surrounding regions. Fig. 6 plots KS test statistics comparing methylation state ("MET") and near-neighbor count ("NBR") distributions at chromatin generations one and three following artificial methylation and demethylation of various nucleosome segments from euchromatin and heterochromatin, respectively. In general, KS test statistics comparing distributions in the artificial region show an initial increase at low artificial segment lengths, followed by a decrease and eventual plateau.

When ~20 nucleosomes are artificially methylated or demethylated, the alteration drives relatively minor changes in chromatin structure. Therefore, as the altered nucleosomes revert to the epigenetic state of their surroundings, minor changes in neighbor count distribution are observed. This is reflected by relatively low KS test statistics comparing neighbor count distributions in the artificial region for short, altered segment lengths. When the methylation state of ~100 nucleosomes is flipped, the alteration causes a

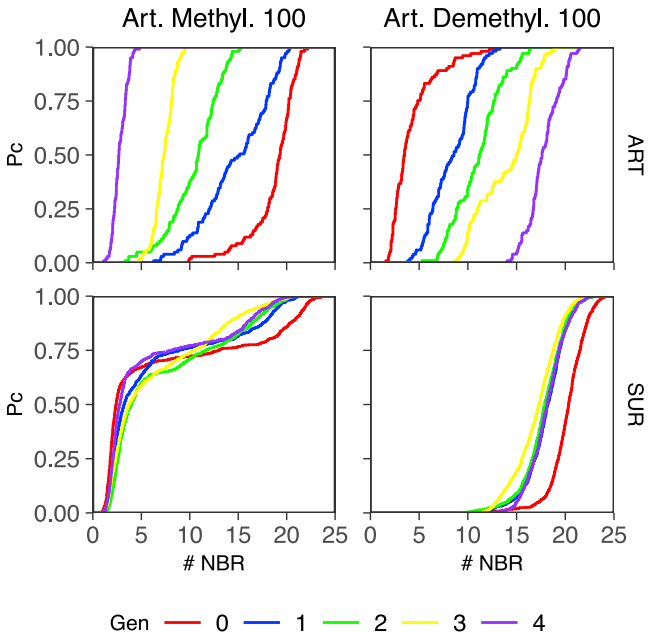

FIGURE 5 For each simulation of a modified chromosome, we isolate a 1000-nucleosome "local" region centered around the artificially methylated or demethylated nucleosome segment. We partition this local region into "artificial" ("ART") and "surrounding" ("SUR") subregions to evaluate patterns in chromatin structure and H3K9me3 profile during four replication cycles. By our labeling convention, we manipulate the H3K9me3 profile at generation zero ("Gen0") and track the effect of this perturbation at generations one ("Gen1") through four ("Gen4"). Here, we plot the distributions of near-neighbor counts in each subregion following artificial methylation and demethylation of 100-nucleosome segments in euchromatin and heterochromatin, respectively. Near-neighbor counts serve as a proxy of chromosome compaction state. For both perturbations to the epigenome, the distributions depict a prominent drift in the near-neighbor counts in the artificial region. Artificially methylated nucleosomes lose neighbors as H3K9me3 modifications become diluted during cell replication, causing a reversion to a loose euchromatin state. Artificially demethylated nucleosomes gain neighbors as H3K9me3 modifications spread from surrounding nucleosomes to reestablish a continuous heterochromatin domain.

transient epigenetic domain opposite to that of the surrounding nucleosomes. This domain is unstable, and high KS test statistics are obtained for both the methylation state and near-neighbor count distributions as the altered nucleosomes equilibrate with their surroundings and restore their original epigenetic states. For artificially methylated or demethylated segments greater than ~200 nucleosomes in length, the alteration is sufficient to introduce a stable domain to the epigenome. Even with mark spreading, nucleosomes in the artificial region maintain their altered identity. This is reflected by relatively low KS test statistics comparing methylation state and neighbor count distributions in the artificial region between chromatin generations one and three.

In general, the KS test statistics obtained from nucleosomes in the surrounding regions are relatively low and increase only slightly with the artificial segment length. These low KS test statistics reflect the stability of the large, continuous epigenetic domains into which we made alterations. The slight increase in KS test statistics at large artificial segment lengths reflects the blurring of the epigenetic boundary between the artificial and surrounding regions caused by methyl spreading.

Epigenetic alterations cause nucleosome migration

Our structural simulations reflect a single chromosome territory containing a condensed heterochromatic core surrounded by a loose euchromatic periphery. Using coordinates of artificially methylated or demethylated nucleosomes in structures predicted by MC simulation, we track nucleosome migration across chromatin generations. We observe that alterations to the epigenome cause a migration of affected nucleosomes toward like phases, such that methylated nucleosomes tend to migrate into the heterochromatic core whereas demethylated nucleosomes tend to migrate toward the euchromatic periphery. The organization of the chromosome into distinct territories and migration of nucleosomes toward like phases recapitulates findings made by Cheng et al. using a phenomenological energy landscape model (61). As mark spreading occurs at boundaries between epigenetic domains, short segments of altered nucleosomes migrate back toward their original phases while restoring their original methylation states (see Fig. 2). By correlating epigenetic sequences and chromatin organization during generations following artificial modification, we demonstrate that small alterations to the epigenome can affect chromatin structure, though their effects tend to be temporary.

DISCUSSION

By applying models of chromatin structure and mark heritability, we simulate the evolution of H3K9me3 marks at four chromatin generations following perturbation to the epigenome. We predict that although loop-mediated mark spreading reverses small alterations to the epigenetic sequence, large changes persist during cell replication. We infer that patterns in epigenetic mark conferral and domain stability are implicated in constitutive heterochromatin repression, embryonic development, and biological aging.

Mark spreading enables broad H3K9me3 coverage

Tandem repeats (short, repeating units of nucleic acid sequences) comprise a sizable portion of mammalian genomes, including ~50–70% of the human genome (67). When unregulated, these repeats express high copy-numbers and destabilize DNA as they randomly rearrange and spread (68). Tandem repeats are also highly susceptible

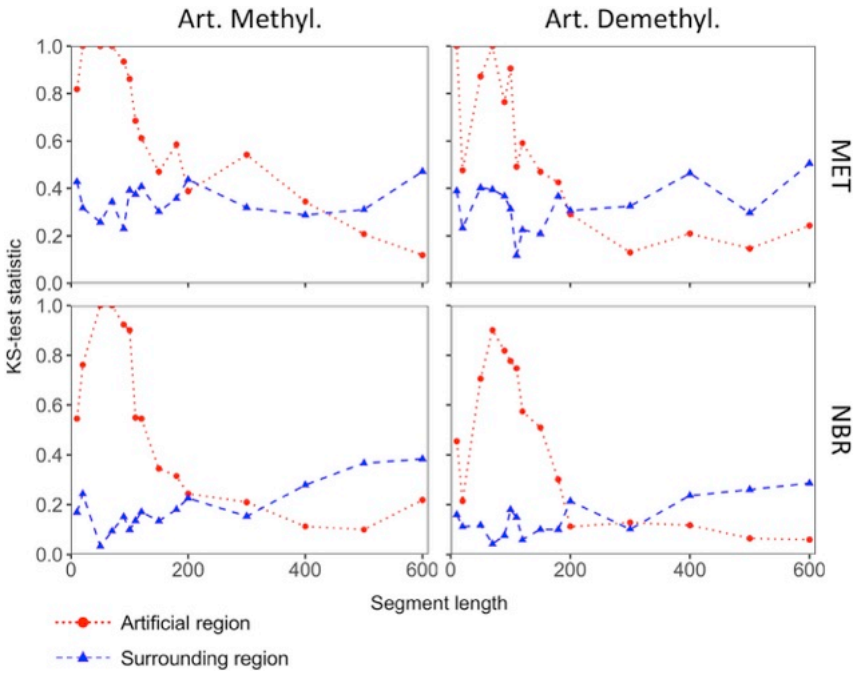

FIGURE 6 From eCDFs like those plotted in Fig. 5, we calculate KS test statistics to quantify changes in the near-neighbor count ("NBR") and H3K9 trimethylation ("MET") profiles as a function of perturbation size ("segment length"). Here, we plot the KS test statistics comparing chromosome generations one and three. We separately determine the KS test statistics for the "artificial" and "surrounding" regions, which contain and linearly neighbor our perturbed nucleosomes, respectively. Test statistics for simulations involving artificial demethylation are obtained from pooled distributions over two trials. For both simulations involving artificial methylation and demethylation, KS test statistics show similar trends with respect to perturbation size. In the artificial region of the chromosome, KS test statistics generally show an initial peak at low perturbation sizes, followed by a gradual plateau. This initial peak corresponds to unstable epigenetic domains prone to switching methylation state to match that of surrounding nucleosomes. The gradual plateau in KS test statistics corresponds to relatively stable epigenetic domains that form due to large perturbations to the epigenome and can persist during chromosomal replication.

to mutations, showing mutation rates up to ~4–7 times that of nonrepeating, gene-rich regions of chromosomal DNA (69). As such, it is advantageous to suppress tandem repeats. A class of heterochromatin known as "constitutive heterochromatin" forms on tandem repeats to shield the regions from biological machinery that replicate and transcribe DNA. Constitutive heterochromatin can be found on key structural components of the chromosome, including the telomeres and pericentromeres (70). H3K9me3 enables the formation of constitutive heterochromatin by promoting HP1 binding and oligomerization, which compact the marked regions of the chromosome. However, constitutive heterochromatin can extend to megabase length scales (68), and this begs the question: how is H3K9me3 deposited across such broad domains?

Our simulations, reflecting loop-mediated mark spreading from H3K9me3-rich regions, complement existing hypotheses of mark establishment on constitutive heterochromatin. One hypothesis of mark establishment states that transcription factor YY1 binds to a subset of tandem repeats, recruiting RNA polymerase to the region. The RNA polymerase transcribes the repeating sequences, forming transcripts that are processed into Piwi-interacting RNAs. Piwi-interacting RNAs are then bound by histone methyltransferase, which deposits the H3K9me3 marks. Because the abundance of YY1 in the cell is insufficient to directly bind all tandem repeats, mark spreading is required for complete coverage of H3K9me3 on constitutive heterochromatin (71). Loop-mediated mark conferral provides one mechanism by which small gaps in methylation mark coverage are filled (see Fig. S2). However, we recognize that based on our simulations, loop-mediated mark conferral cannot explain H3K9me3 spreading across sparsely methylated regions, and for this our results suggest there must be some more active biological driving force.

Dynamic patterns of epigenetic modifications support embryonic development

A dynamic profile of H3K9me3 modifications is a hallmark of cellular differentiation. In addition to its primary role in condensing constitutive heterochromatin, H3K9me3 is also thought to regulate gene-rich "facultative heterochromatin" during embryonic development. The heterochromatin mark is implicated in repression of developmental regulatory genes in embryonic stem cells, and removal of the H3K9 methyltransferases that establish the mark has been linked to aberrant cell differentiation. Once cell differentiation is initiated, H3K9me3 marks become enriched on pluripotency and lineage-inappropriate genes to drive the cell toward its final somatic cell state. Over time, H3K9me3 marks become less prominent in gene-rich regions (72). Our simulations portray loop-mediated epigenetic mark conferral as a passive mechanism allowing for the dynamic patterns of H3K9me3 during embryonic development. Results from our models capture the dispersion of short, methylated domains within a few cell cycles, as is expected on gene promoters extending just a few nucleosomes in length.

The transient modification of short heterochromatin domains observed in simulations is also consistent with transposon suppression during embryonic development (73–75).

Transposons, or so-called "jumping genes," are short repeating elements of the genome that can move between loci if unregulated. These sequences affect gene expression by signaling for transcription factors and chromatin modifiers (73). As with the tandem repeats found in constitutive heterochromatin, the repeating sequences of transposons destabilize DNA, making physical regulation of transposons biologically favorable. During early embryonic development, DNA is globally unmethylated, and suppression of transposons is attributed predominantly to H3K9me3 and other chromatin modifications until DNA methylation is established (73,75,76). The prevalence of H3K9me3 modifications is observed to decrease during the first few cell divisions (77,78). Ultimately, DNA methylation takes over as the predominant repressor of transposons in somatic cells (75). Our simulations suggest that loop-mediated mark spreading contributes to a passive switch in the dominant mechanism of transposon repression during progressive stages of embryonic development. H3K9me3-rich domains are unstable at short segment lengths and are therefore unsuitable for long-term transposon suppression.

Drift at epigenetic boundaries contributes to biological aging

Epigenetic drift occurs as small changes in the epigenome accumulate over time following cell replication (79). The physical mechanisms underlying epigenetic drift remain unclear, and effects on patterns of H3K9me3 modifications vary by organism (80,81). In humans, aging has been associated with both enrichment and reduction of H3K9me3 marks. Age-related changes in H3K9me3 coverage result in aberrant gene expression and can contribute to tumor formation (82). Our models capture the effects of epigenetic drift at the interface of heterochromatic and euchromatic domains. We observe the spreading of H3K9me3 marks from methylated heterochromatin to unmethylated euchromatin, affecting chromatin compression near the domain boundary. For example, epigenetic drift is prominent in simulations following artificial demethylation of 600 nucleosomes, where heterochromatic domains creep into euchromatic regions even after just four cell generations (see Fig. S3). This epigenetic drift blurs the separation between gene-active euchromatin and silenced heterochromatin, as reflected by a smoothing of the neighbor count profiles near epigenetic boundaries. By capturing characteristic features of epigenetic drift using physics-based simulation, we conclude that mark conferral caused by chromatin looping contributes to the breakdown of epigenetic boundaries over time, potentially leading to phenotypic effects of aging.

CONCLUSIONS

Using a physical model rooted in polymer theory, we capture observed biological phenomena at resolutions inaccessible from the bench-top. In this work, we predict H3K9me3 stability between chromatin generations by iterating between an MC structural simulation and a kinetic model of loop-mediated mark conferral. Results from our simulations suggest that mark spreading reverses small perturbations to the epigenome, whereas larger changes greater than 100–200 nucleosomes in length persist through multiple cell generations.

By relating observations from our simulations to known biological functions of H3K9me3, we assert that mark spreading at epigenetic boundaries contributes to broad coverage of H3K9me3 in constitutive heterochromatin. The switching of small epigenetic domains observed in our simulations is also consistent with the dynamic patterns of H3K9me3 observed during cell differentiation and transposon suppression. Finally, our simulations demonstrate that boundaries between heterochromatin and euchromatin domains tend to blur, drifting over time because of chromatin looping and associated mark conferral.

Based on these observations, we conclude that epigenetic drift caused by chromatin looping is connected to biological aging and cancer growth later in life. Although further studies are required to elucidate mechanisms of H3K9me3 mark establishment in sparsely methylated regions, this work poses loop-mediated mark conferral as a potential mechanism regulating gene expression at various stages of life.

SUPPORTING MATERIAL

Supporting material can be found online at https://doi.org/10.1016/j.bpj.2021.10.019.

AUTHOR CONTRIBUTIONS

J.G.W. designed research, conducted research, and wrote the article. S.H.S. designed research, conducted research, and wrote the article. A.J.S. designed research and wrote the article.

ACKNOWLEDGMENTS

Financial support for this work is provided by National Institutes of Health, NIH-4D Nucleome Program,and National Science Foundation, Physics of Living Systems Program (PHY-2102726). S.H.S. acknowledges funding support from the National Science Foundation, NSF Graduate Fellowship Program (DGE-1656518).

REFERENCES

1. Moss, T. J., and L. L. Wallrath. 2007. Connections between epigenetic gene silencing and human disease. *Mutat. Res.* 618:163–174.
2. Nguyen-Ba, G., and P. Vasseur. 1999. Epigenetic events during the process of cell transformation induced by carcinogens (review). *Oncol. Rep.* 6:925–932.
3. Egger, G., G. Liang, …, P. A. Jones. 2004. Epigenetics in human disease and prospects for epigenetic therapy. *Nature.* 429:457–463.

4. Peters, A. H., J. E. Mermoud, …, T. Jenuwein. 2002. Histone H3 lysine 9 methylation is an epigenetic imprint of facultative heterochromatin. *Nat. Genet.* 30:77–80.
5. Magklara, A., A. Yen, …, S. Lomvardas. 2011. An epigenetic signature for monoallelic olfactory receptor expression. *Cell.* 145:555–570.
6. Matsui, T., D. Leung, …, Y. Shinkai. 2010. Proviral silencing in embryonic stem cells requires the histone methyltransferase ESET. *Nature.* 464:927–931.
7. Nielsen, S. J., R. Schneider, …, T. Kouzarides. 2001. Rb targets histone H3 methylation and HP1 to promoters. *Nature.* 412:561–565.
8. Bannister, A. J., P. Zegerman, …, T. Kouzarides. 2001. Selective recognition of methylated lysine 9 on histone H3 by the HP1 chromo domain. *Nature.* 410:120–124.
9. Lachner, M., D. O'Carroll, …, T. Jenuwein. 2001. Methylation of histone H3 lysine 9 creates a binding site for HP1 proteins. *Nature.* 410:116–120.
10. Nakayama, J., J. C. Rice, …, S. I. Grewal. 2001. Role of histone H3 lysine 9 methylation in epigenetic control of heterochromatin assembly. *Science.* 292:110–113.
11. Canzio, D., E. Y. Chang, …, B. Al-Sady. 2011. Chromodomain-mediated oligomerization of HP1 suggests a nucleosome-bridging mechanism for heterochromatin assembly. *Mol. Cell.* 41:67–81.
12. Verschure, P. J., I. van der Kraan, …, R. van Driel. 2005. In vivo HP1 targeting causes large-scale chromatin condensation and enhanced histone lysine methylation. *Mol. Cell. Biol.* 25:4552–4564.
13. Fritsch, L., P. Robin, …, S. Ait-Si-Ali. 2010. A subset of the histone H3 lysine 9 methyltransferases Suv39h1, G9a, GLP, and SETDB1 participate in a multimeric complex. *Mol. Cell.* 37:46–56.
14. Peters, A. H., S. Kubicek, …, T. Jenuwein. 2003. Partitioning and plasticity of repressive histone methylation states in mammalian chromatin. *Mol. Cell.* 12:1577–1589.
15. Rea, S., F. Eisenhaber, …, T. Jenuwein. 2000. Regulation of chromatin structure by site-specific histone H3 methyltransferases. *Nature.* 406:593–599.
16. Le, T. B., M. V. Imakaev, …, M. T. Laub. 2013. High-resolution mapping of the spatial organization of a bacterial chromosome. *Science.* 342:731–734.
17. Rao, S. S., M. H. Huntley, …, E. L. Aiden. 2014. A 3D map of the human genome at kilobase resolution reveals principles of chromatin looping. *Cell.* 159:1665–1680.
18. Annunziato, A. T. 2005. Split decision: what happens to nucleosomes during DNA replication? *J. Biol. Chem.* 280:12065–12068.
19. Xu, M., W. Wang, …, B. Zhu. 2011. A model for mitotic inheritance of histone lysine methylation. *EMBO Rep.* 13:60–67.
20. Alabert, C., T. K. Barth, …, A. Groth. 2015. Two distinct modes for propagation of histone PTMs across the cell cycle. *Genes Dev.* 29:585–590.
21. Dodd, I. B., M. A. Micheelsen, …, G. Thon. 2007. Theoretical analysis of epigenetic cell memory by nucleosome modification. *Cell.* 129:813–822.
22. Micheelsen, M. A., N. Mitarai, …, I. B. Dodd. 2010. Theory for the stability and regulation of epigenetic landscapes. *Phys. Biol.* 7:026010.
23. Zhang, H., X.-J. Tian, …, J. Xing. 2014. Statistical mechanics model for the dynamics of collective epigenetic histone modification. *Phys. Rev. Lett.* 112:068101.
24. Tian, X.-J., H. Zhang, …, J. Xing. 2016. Achieving diverse and monoallelic olfactory receptor selection through dual-objective optimization design. *Proc. Natl. Acad. Sci. USA.* 113:E2889–E2898.
25. Erdel, F., and E. C. Greene. 2016. Generalized nucleation and looping model for epigenetic memory of histone modifications. *Proc. Natl. Acad. Sci. USA.* 113:E4180–E4189.
26. Michieletto, D., E. Orlandini, and D. Marenduzzo. 2016. Polymer model with epigenetic recoloring reveals a pathway for the de novo establishment and 3D organization of chromatin domains. *Phys. Rev. X.* 6:041047.
27. Michieletto, D., M. Chiang, …, D. Marenduzzo. 2018. Shaping epigenetic memory via genomic bookmarking. *Nucleic Acids Res.* 46:83–93.
28. Dodd, I. B., and K. Sneppen. 2011. Barriers and silencers: a theoretical toolkit for control and containment of nucleosome-based epigenetic states. *J. Mol. Biol.* 414:624–637.
29. Jost, D., and C. Vaillant. 2018. Epigenomics in 3D: importance of long-range spreading and specific interactions in epigenomic maintenance. *Nucleic Acids Res.* 46:2252–2264.
30. Erdel, F., K. Müller-Ott, and K. Rippe. 2013. Establishing epigenetic domains via chromatin-bound histone modifiers. *Ann. N. Y. Acad. Sci.* 1305:29–43.
31. Sandholtz, S. H., Q. MacPherson, and A. J. Spakowitz. 2020. Physical modeling of the heritability and maintenance of epigenetic modifications. *Proc. Natl. Acad. Sci. USA.* 117:20423–20429.
32. Sneppen, K., and I. B. Dodd. 2012. A simple histone code opens many paths to epigenetics. *PLoS Comput. Biol.* 8:e1002643.
33. Zerihun, M. B., C. Vaillant, and D. Jost. 2015. Effect of replication on epigenetic memory and consequences on gene transcription. *Phys. Biol.* 12:026007.
34. Feser, J., and J. Tyler. 2011. Chromatin structure as a mediator of aging. *FEBS Lett.* 585:2041–2048.
35. Tsurumi, A., and W. X. Li. 2012. Global heterochromatin loss: a unifying theory of aging? *Epigenetics.* 7:680–688.
36. Haithcock, E., Y. Dayani, …, J. Liu. 2005. Age-related changes of nuclear architecture in *Caenorhabditis elegans*. *Proc. Natl. Acad. Sci. USA.* 102:16690–16695.
37. Larson, K., S.-J. Yan, …, W. X. Li. 2012. Heterochromatin formation promotes longevity and represses ribosomal RNA synthesis. *PLoS Genet.* 8:e1002473.
38. Zhang, W., J. Li, …, J. C. Belmonte. 2015. Aging stem cells. A Werner syndrome stem cell model unveils heterochromatin alterations as a driver of human aging. *Science.* 348:1160–1163.
39. Shumaker, D. K., T. Dechat, …, R. D. Goldman. 2006. Mutant nuclear lamin A leads to progressive alterations of epigenetic control in premature aging. *Proc. Natl. Acad. Sci. USA.* 103:8703–8708.
40. Villeponteau, B. 1997. The heterochromatin loss model of aging. *Exp. Gerontol.* 32:383–394.
41. Wood, J. G., S. Hillenmeyer, …, S. L. Helfand. 2010. Chromatin remodeling in the aging genome of Drosophila. *Aging Cell.* 9:971–978.
42. MacPherson, Q., B. Beltran, and A. J. Spakowitz. 2018. Bottom-up modeling of chromatin segregation due to epigenetic modifications. *Proc. Natl. Acad. Sci. USA.* 115:12739–12744.
43. Sandholtz, S., B. Beltran, and A. Spakowitz. 2019. Physical modeling of the spreading of epigenetic modifications through transient DNA looping. *J. Phys. A Math. Theor.* 52:434001.
44. Feodorova, Y., M. Falk, …, I. Solovei. 2020. Viewing nuclear architecture through the eyes of nocturnal mammals. *Trends Cell Biol.* 30:276–289.
45. Koslover, E. F., and A. J. Spakowitz. 2013. Systematic coarse-graining of microscale polymer models as effective elastic chains. *Macromolecules.* 46:2003–2014.
46. Koslover, E. F., and A. J. Spakowitz. 2013. Discretizing elastic chains for coarse-grained polymer models. *Soft Matter.* 29:7016–7027.
47. Koslover, E. F., and A. J. Spakowitz. 2014. Multiscale dynamics of semiflexible polymers from a universal coarse-graining procedure. *Phys. Rev. E Stat. Nonlin. Soft Matter Phys.* 90:013304.
48. Cremer, T., and C. Cremer. 2001. Chromosome territories, nuclear architecture and gene regulation in mammalian cells. *Nat. Rev. Genet.* 2:292–301.
49. Pike, D. Q., F. A. Detcheverry, …, J. J. de Pablo. 2009. Theoretically informed coarse grain simulations of polymeric systems. *J. Chem. Phys.* 131:084903.
50. Hathaway, N. A., O. Bell, …, G. R. Crabtree. 2012. Dynamics and memory of heterochromatin in living cells. *Cell.* 149:1447–1460.

51. Hodges, C., and G. R. Crabtree. 2012. Dynamics of inherently bounded histone modification domains. *Proc. Natl. Acad. Sci. USA.* 109:13296–13301.

52. Mulligan, P. J., E. F. Koslover, and A. J. Spakowitz. 2015. Thermodynamic model of heterochromatin formation through epigenetic regulation. *J. Phys. Condens. Matter.* 27:064109.

53. Arya, G., and T. Schlick. 2006. Role of histone tails in chromatin folding revealed by a mesoscopic oligonucleosome model. *Proc. Natl. Acad. Sci. USA.* 103:16236–16241.

54. Nuebler, J., G. Fudenberg, …, L. A. Mirny. 2018. Chromatin organization by an interplay of loop extrusion and compartmental segregation. *Proc. Natl. Acad. Sci. USA.* 115:E6697–E6706.

55. Barbieri, M., M. Chotalia, …, M. Nicodemi. 2012. Complexity of chromatin folding is captured by the strings and binders switch model. *Proc. Natl. Acad. Sci. USA.* 109:16173–16178.

56. Chiariello, A. M., C. Annunziatella, …, M. Nicodemi. 2016. Polymer physics of chromosome large-scale 3D organisation. *Sci. Rep.* 6:29775.

57. Di Pierro, M., B. Zhang, …, J. N. Onuchic. 2016. Transferable model for chromosome architecture. *Proc. Natl. Acad. Sci. USA.* 113:12168–12173.

58. Di Pierro, M., R. R. Cheng, …, J. N. Onuchic. 2017. De novo prediction of human chromosome structures: epigenetic marking patterns encode genome architecture. *Proc. Natl. Acad. Sci. USA.* 114:12126–12131.

59. Falk, M., Y. Feodorova, …, L. A. Mirny. 2019. Heterochromatin drives compartmentalization of inverted and conventional nuclei. *Nature.* 570:395–399.

60. MacPherson, Q., B. Beltran, and A. J. Spakowitz. 2020. Chromatin compaction leads to a preference for peripheral heterochromatin. *Biophys. J.* 118:1479–1488.

61. Cheng, R. R., V. G. Contessoto, …, J. N. Onuchic. 2020. Exploring chromosomal structural heterogeneity across multiple cell lines. *eLife.* 9:e60312.

62. ENCODE Project Consortium. 2012. An integrated encyclopedia of DNA elements in the human genome. *Nature.* 489:57–74.

63. Bernstein, B. 2010. GM12878 H3K9me3 histone mods by ChIP-seq signal from ENCODE/Broad. hgdownload.soe.ucsc.edu/goldenPath/hg19/encodeDCC/wgEncodeBroadHistone/wgEncodeBroadHistoneGm12878H3k9me3StdSig.bigWig. Accessed October 28, 2017.

64. Zee, B. M., R. S. Levin, …, B. A. Garcia. 2010. *In vivo* residue-specific histone methylation dynamics. *J. Biol. Chem.* 285:3341–3350.

65. Patnaik, D., H. G. Chin, …, S. Pradhan. 2004. Substrate specificity and kinetic mechanism of mammalian G9a histone H3 methyltransferase. *J. Biol. Chem.* 279:53248–53258.

66. Ghosh, R. P., J. M. Franklin, …, J. T. Liphardt. 2019. A fluorogenic array for temporally unlimited single-molecule tracking. *Nat. Chem. Biol.* 15:401–409.

67. Lu, J. Y., W. Shao, …, X. Shen. 2020. Genomic repeats categorize genes with distinct functions for orchestrated regulation. *Cell Rep.* 30:3296–3311.e5.

68. Becker, J. S., D. Nicetto, and K. S. Zaret. 2016. H3K9me3-dependent heterochromatin: barrier to cell fate changes. *Trends Genet.* 32:29–41.

69. Fan, H., and J.-Y. Chu. 2007. A brief review of short tandem repeat mutation. *Genomics Proteomics Bioinformatics.* 5:7–14.

70. Saksouk, N., E. Simboeck, and J. Déjardin. 2015. Constitutive heterochromatin formation and transcription in mammals. *Epigenetics Chromatin.* 8:3.

71. Kim, J., and H. Kim. 2012. Recruitment and biological consequences of histone modification of H3K27me3 and H3K9me3. *ILAR J.* 53:232–239.

72. Nicetto, D., and K. S. Zaret. 2019. Role of H3K9me3 heterochromatin in cell identity establishment and maintenance. *Curr. Opin. Genet. Dev.* 55:1–10.

73. He, J., X. Fu, …, A. P. Hutchins. 2019. Transposable elements are regulated by context-specific patterns of chromatin marks in mouse embryonic stem cells. *Nat. Commun.* 10:34.

74. Zhang, T., S. Cooper, and N. Brockdorff. 2015. The interplay of histone modifications - writers that read. *EMBO Rep.* 16:1467–1481.

75. Walter, M., A. Teissandier, …, D. Bourc'his. 2016. An epigenetic switch ensures transposon repression upon dynamic loss of DNA methylation in embryonic stem cells. *eLife.* 5:e11418.

76. Messerschmidt, D. M., B. B. Knowles, and D. Solter. 2014. DNA methylation dynamics during epigenetic reprogramming in the germline and preimplantation embryos. *Genes Dev.* 28:812–828.

77. Burton, A., and M.-E. Torres-Padilla. 2014. Chromatin dynamics in the regulation of cell fate allocation during early embryogenesis. *Nat. Rev. Mol. Cell Biol.* 15:723–734.

78. van Kruijsbergen, I., S. Hontelez, …, G. J. C. Veenstra. 2017. Heterochromatic histone modifications at transposons in Xenopus tropicalis embryos. *Dev. Biol.* 426:460–471.

79. Mendelsohn, A. R., and J. W. Larrick. 2017. Epigenetic drift is a determinant of mammalian lifespan. *Rejuvenation Res.* 20:430–436.

80. Ma, Z., H. Wang, …, N. Liu. 2018. Epigenetic drift of H3K27me3 in aging links glycolysis to healthy longevity in *Drosophila*. *eLife.* 7:e35368.

81. McCauley, B. S., and W. Dang. 2014. Histone methylation and aging: lessons learned from model systems. *Biochim. Biophys. Acta.* 1839:1454–1462.

82. Sidler, C., O. Kovalchuk, and I. Kovalchuk. 2017. Epigenetic regulation of cellular senescence and aging. *Front. Genet.* 8:138.